Triazatruxene based star-shaped thermally activated delayed fluorescence emitters: modulating the performance of solution-processed non-doped OLEDs via side-group engineering

Suraj Kumar Pathak,[a,b] He Liu,[a*]Changjiang Zhou,[a] Guohua Xie,[c*] Chuluo Yang[a,c*]

[a] *Shenzhen Key Laboratory of Polymer Science and Technology, College of Materials Science and Engineering, Shenzhen University, Shenzhen 518060, P. R. China.* *liuhe001@szu.edu.cn,clyang@szu.edu.cn.*

[b] *Key Laboratory of Optoelectronic Devices and Systems of Ministry of Education and Guangdong Province, College of Optoelectronic Engineering, Shenzhen University, Shenzhen 518060, P. R. China.*

[c] *Hubei Key Lab on Organic and Polymeric Optoelectronic Materials, Department of Chemistry, Wuhan University, Wuhan, 430072, P. R. China. guohua.xie@whu.edu.cn.*

General information

All oxygen- and moisture-sensitive manipulations were carried out under an inert atmosphere. All the chemicals were purchased from commercial sources and used as received unless stated otherwise. Toluene was refluxed over Na and distilled under dry argon. The 500 MHz ^{1}H and 125MHz ^{13}C NMR spectra were recorded on a Bruker Ascend 500 spectrometer using $CDCl_3$ and DMSO-D_6 as solvent and tetramethylsilane (TMS) as an internal reference. High-resolution electrospray (ESI) mass spectra were performed on SCIEX TripleTOF6600 nano LCMS. UV-Vis absorption spectra were recorded on a Shimadzu UV-2700 recording spectrophotometer. Photoluminescence (PL) spectra were recorded on a Hitachi F-4600 fluorescence spectrophotometer. Phosphorescence spectra of thin films were conducted at 77K. Thermogravimetric analysis (TGA) was recorded on a TA Q50 instrument under nitrogen atmosphere at a heating rate of 10^{o}C/min from 25 to 800 ^{o}C. The temperature of degradation (T_d) was correlated to a 5% weight loss. Differential Scanning Calorimetry were carried out on a TA Q200. The glass transition temperature (T_g) was determined from the second heating scan at a heating rate of 10^{o}C min^{-1} from 25 to 250 ^{o}C.

Cyclic voltammetry (CV) was carried out in nitrogen-purged tetrahydrofuran or acetonitrile (reduction scan) or dichloromethane (oxidation scan) at room temperature with a CHI voltammetric analyzer. Tetrabutylammoniumhexafluorophosphate (0.1 M) was used as the supporting electrolyte. The conventional three-electrode configuration consisted of a platinum working electrode, a platinum wire auxiliary electrode and an Ag wire pseudo-reference electrode with ferrocenium ferrocene (Fc^+/Fc) as the internal standard. Cyclic voltammograms were obtained at scan rate of 100 mV/s. Formal potentials were calculated as the average of cyclic voltammetric anodic and cathodic peaks. The HOMO energy levels of the compounds were calculated according to the formula: $-[4.8 + (E_{1/2(ox/red)} - E_{1/2(Fc/Fc+)})]$ eV. The onset potential was determined from the intersection of two tangents drawn at the rising and background current of the cyclic voltammogram. The PL lifetimes were measured by a single photon counting spectrometer from Edinburgh Instruments (FLS920) with a Picosecond Pulsed UV-LASTER (LASTER377) as the excitation source. The samples were placed in a vacuum cryostat chamber with the temperature control. The solid state absolute PLQYs were measured on a Quantaurus - QY measurement system (C9920-02, Hamamatsu Photonics) equipped with a calibrated integrating sphere in the host of mCP (5 wt%) and all the samples were excited at 342 nm. During the PLQY measurements, the integrating sphere was purged with pure and dry argon to maintain an inert environment. The ground state and excited states molecular structures were optimized at the B3LYP-D3(BJ)/def2-SVP and PBE0/def2-SVP respectively.

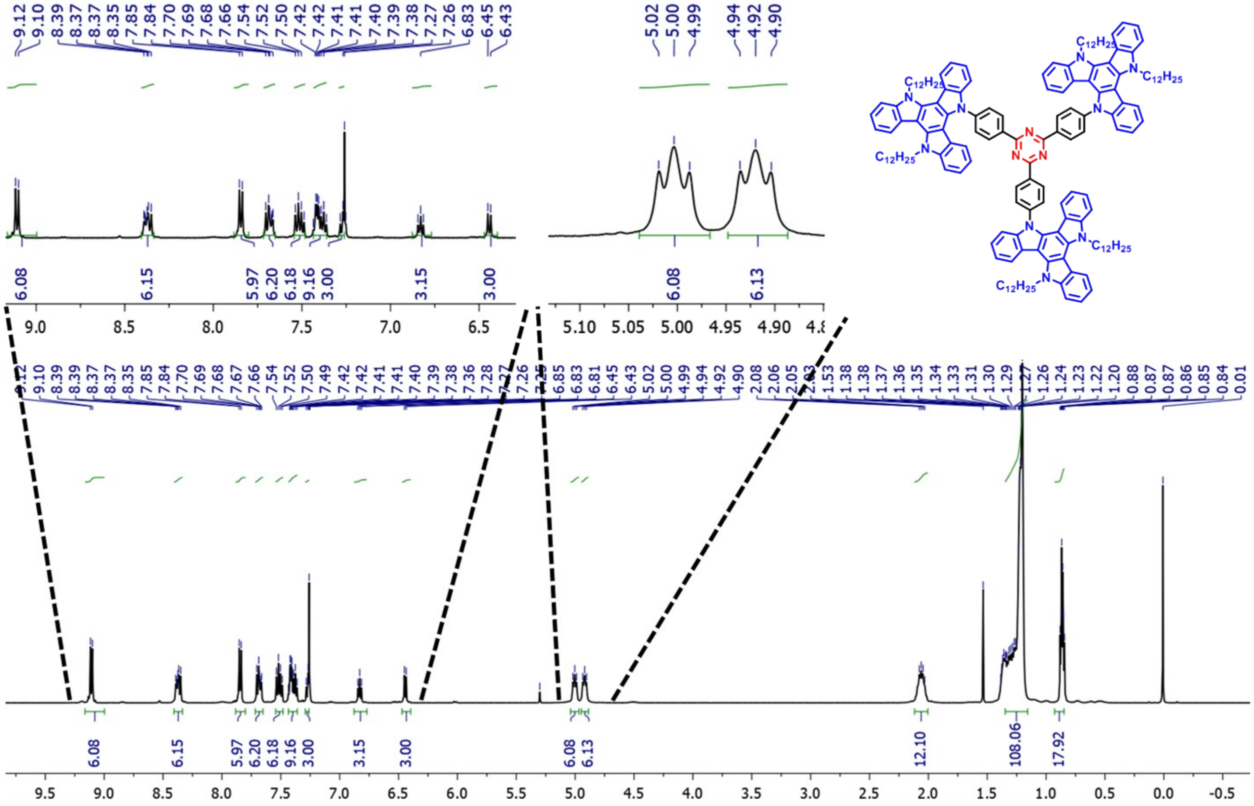

Figure S1. ^{1}H NMR spectrum of **TATC-TRZ** in $CDCl_3$ (500 MHz, 25 °C).

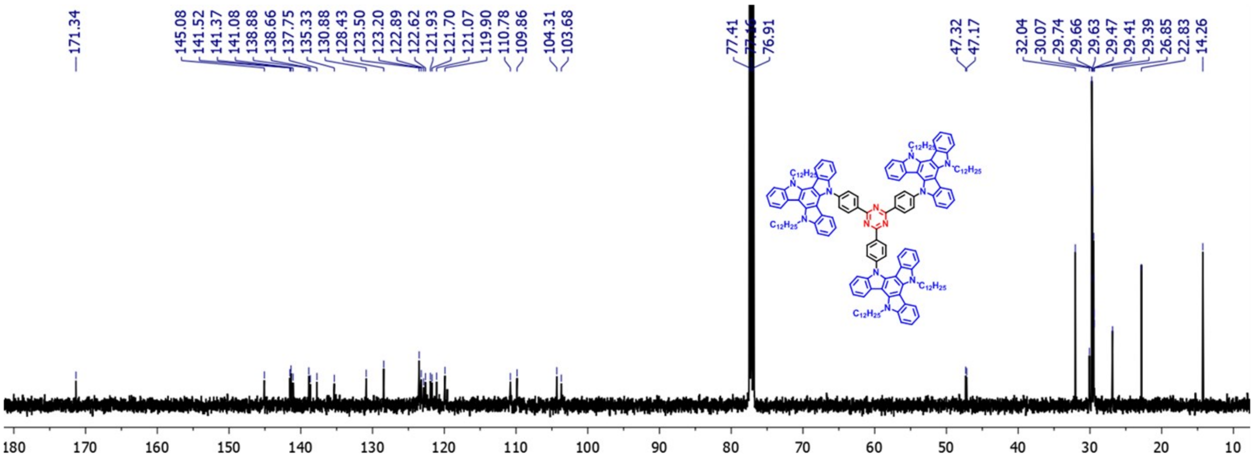

Figure S2. ^{13}C NMR spectrum of **TATC-TRZ** in $CDCl_3$ (125 MHz, 25 °C).

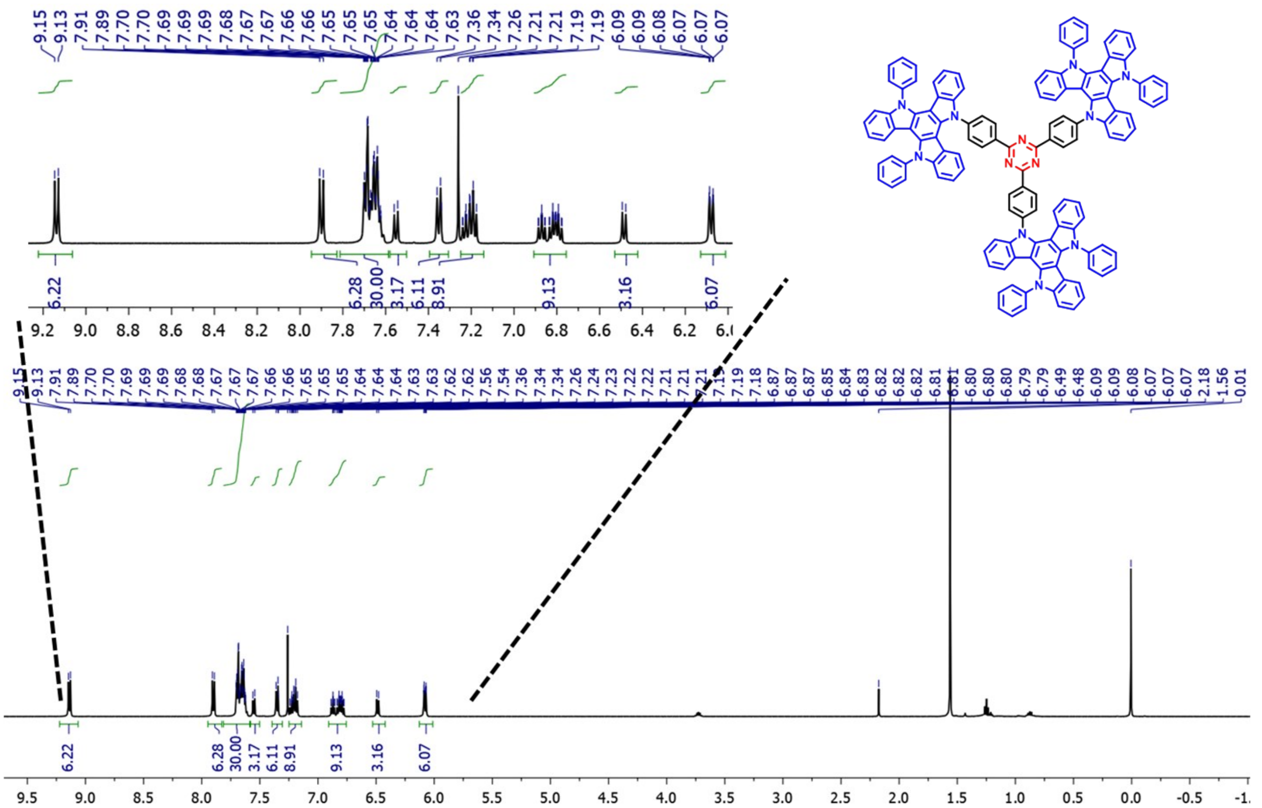

Figure S3. ^{1}H NMR spectrum of **TATP-TRZ** in $CDCl_3$ (500 MHz, 25 °C).

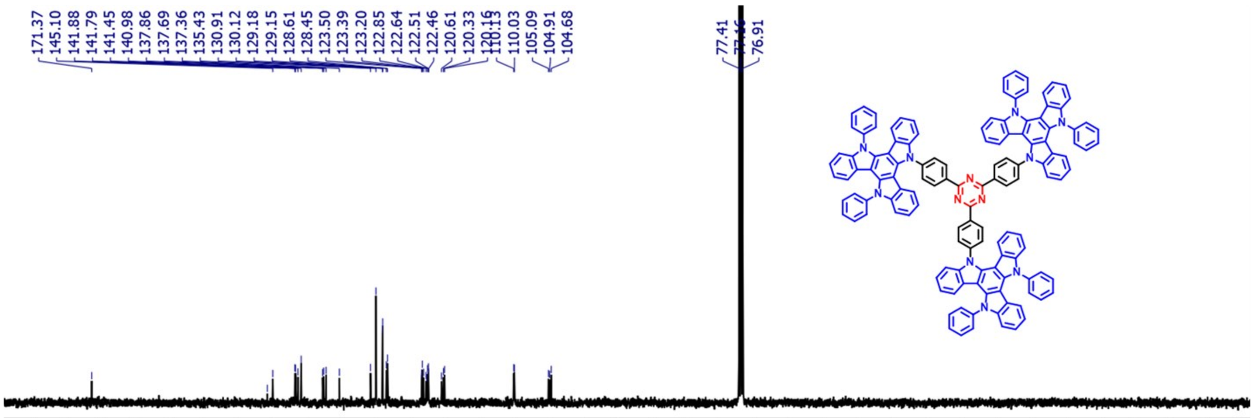

Figure S4. ^{13}C NMR spectrum of **TATP-TRZ** in $CDCl_3$ (125 MHz, 25 °C).

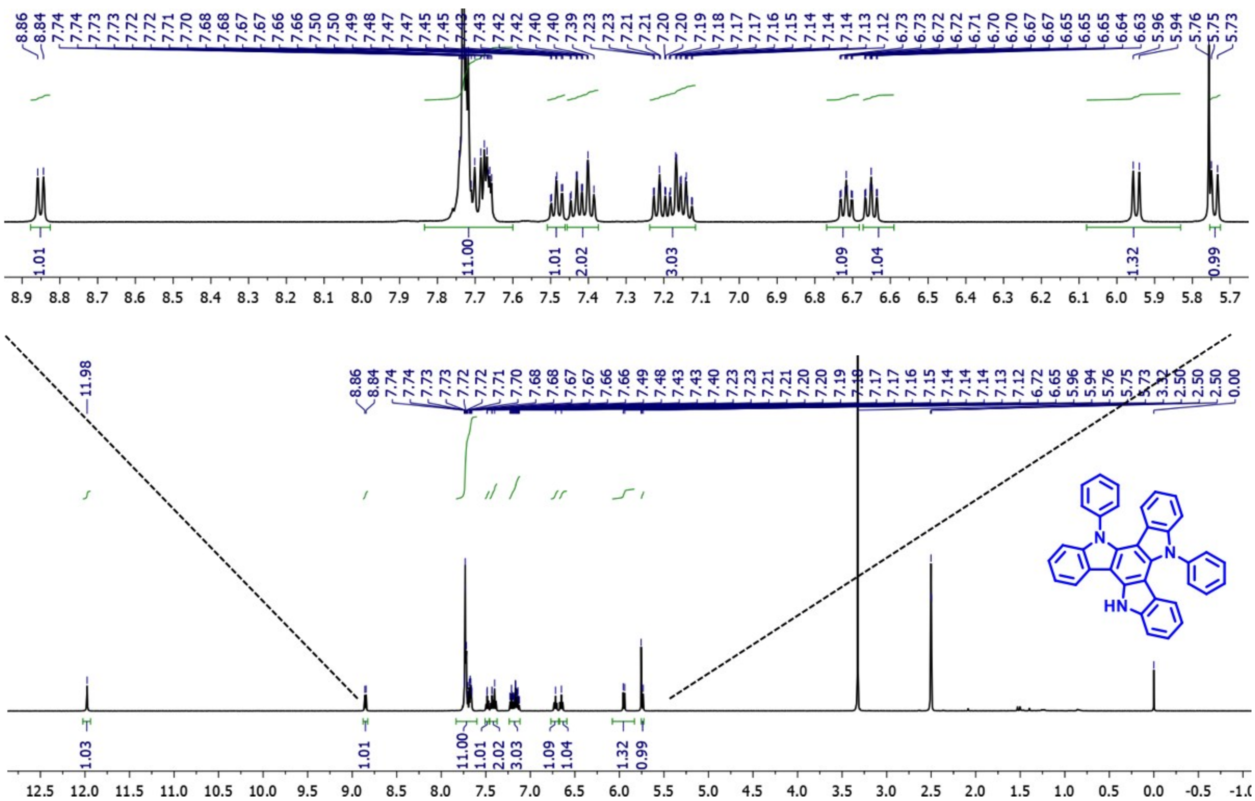

Figure S5. ^{1}H NMR spectrum of **TATP** in DMSO-D$_6$ (500 MHz, 25 °C).

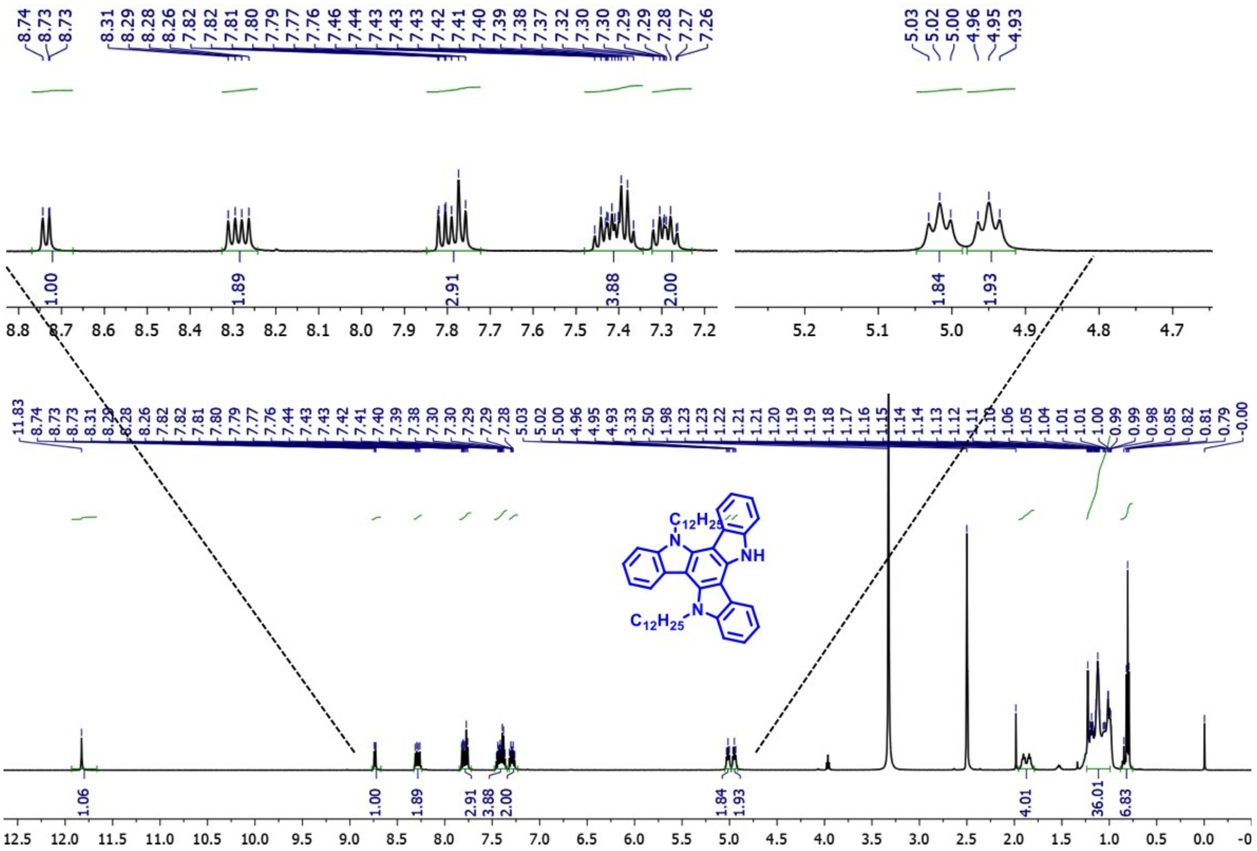

Figure S6. ^{1}H NMR spectrum of **TATP** in DMSO-D$_6$ (500 MHz, 25 °C).

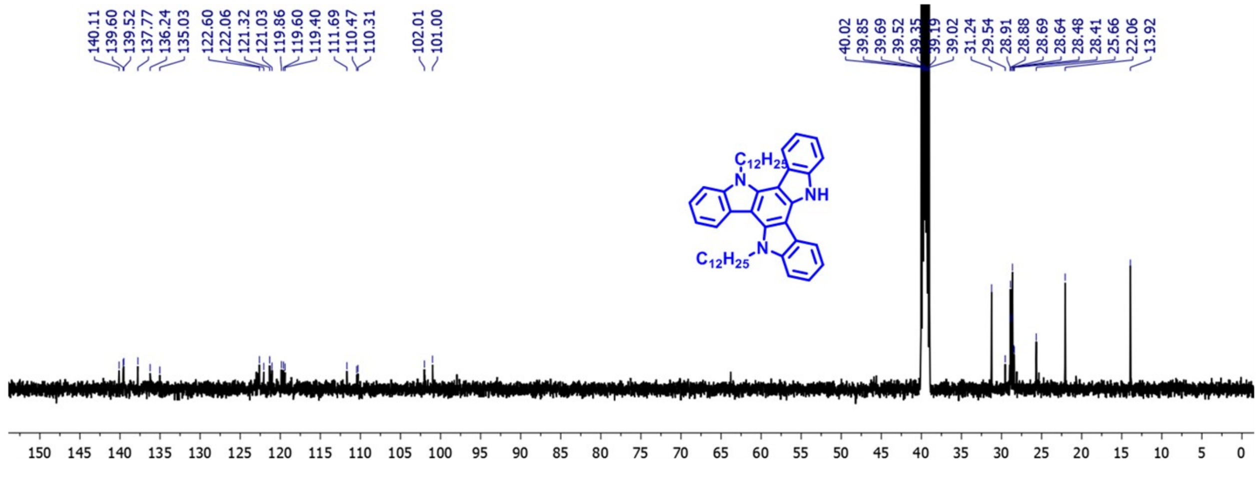

Figure S7. ^{13}C NMR spectrum of **TATC** in DMSO-D$_6$ (125 MHz, 25 °C).

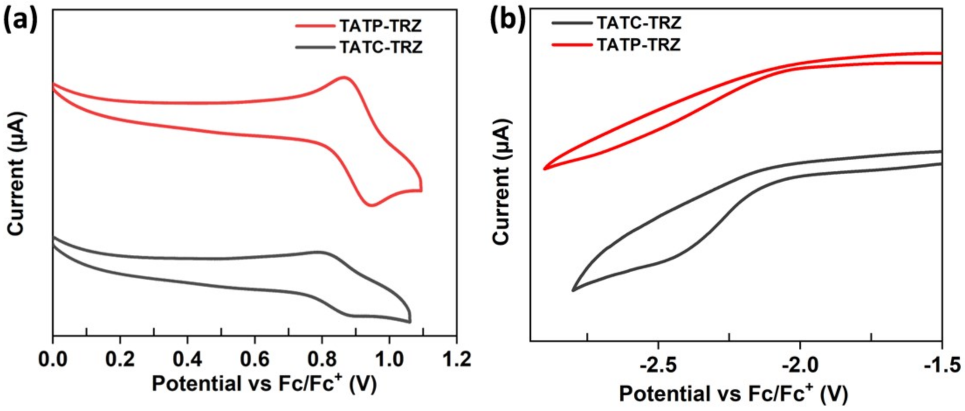

Figure S8. (a) Cyclic voltammograms of **TATC-TRZ** and **TATP-TRZ** in 0.1M $TBAPF_6$ dichloromethane (for the oxidation process); (b) and DMF (for the reduction process) solutions.

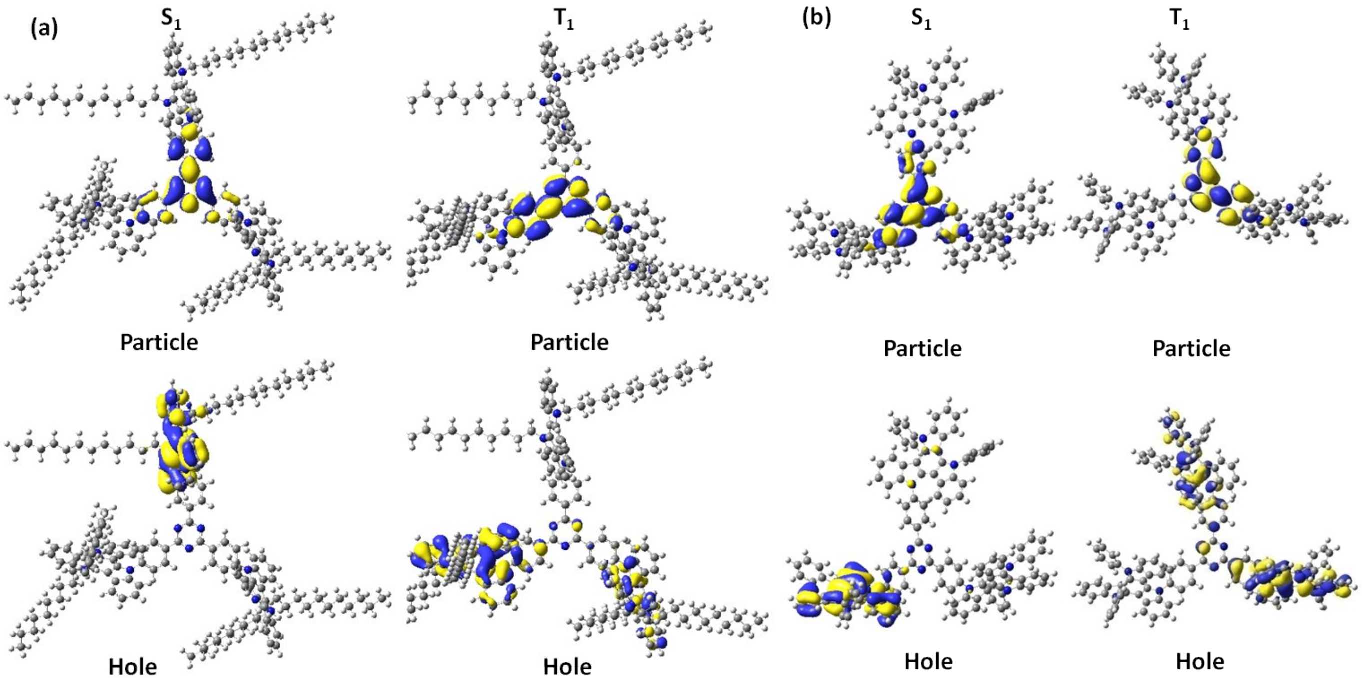

Figure S9. Natural transition orbitals (NTOs) of the hole-particle contribution for (a) **TATC-TRZ** and (b) **TATP-TRZ** at S_1 and T_1 excited state.

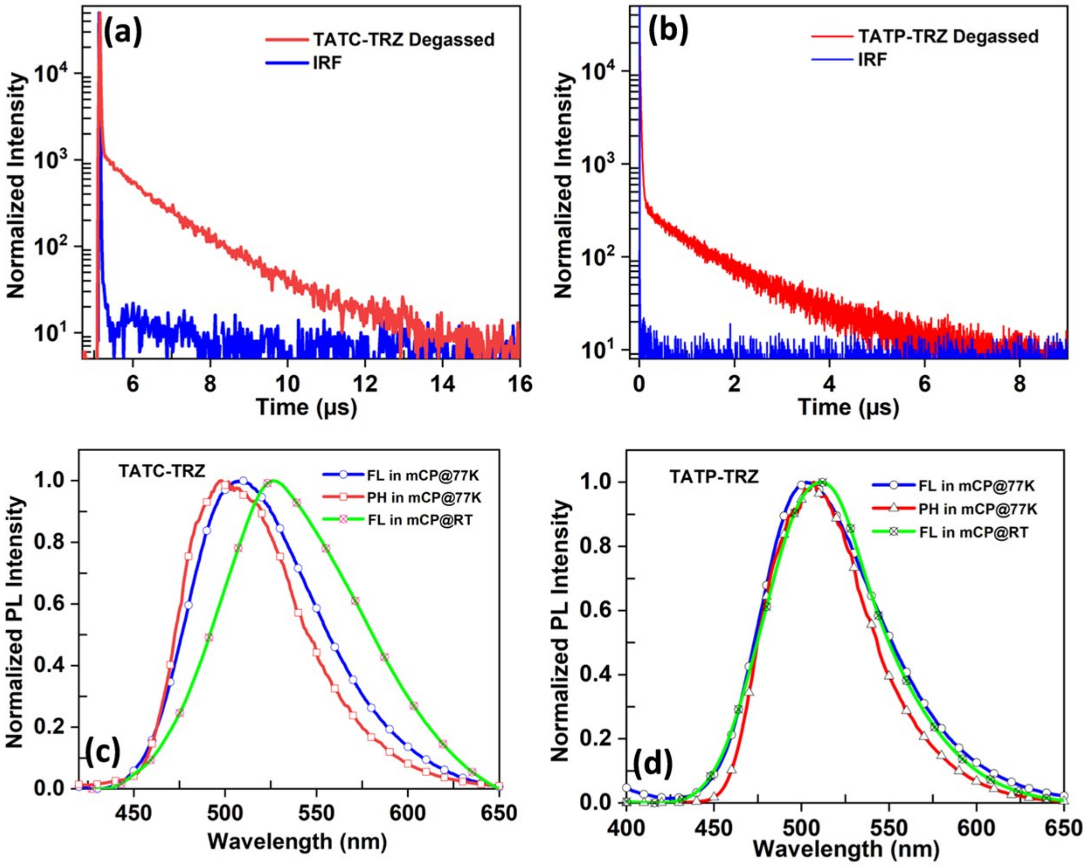

Figure S10. Transient photoluminescence decay curves of (a) **TATC-TRZ**, (b) **TATP-TRZ** in mCP (5 wt% of emitter) doped film under oxygen free condition. Fluorescence spectra both at 300 K and 77 K and Phosphorescence spectra at 77K of (c) **TATC-TRZ** and (d) **TATP-TRZ** in mCP (5 wt% of emitter) doped film.

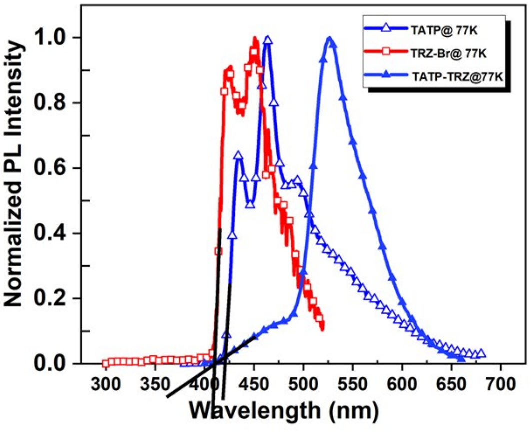

Figure S11. Phosphorescence spectra at 77 K of **TATP (donor)**, **TRZ-Br (acceptor)** and **TATP-TRZ (emitter)** in neat film.

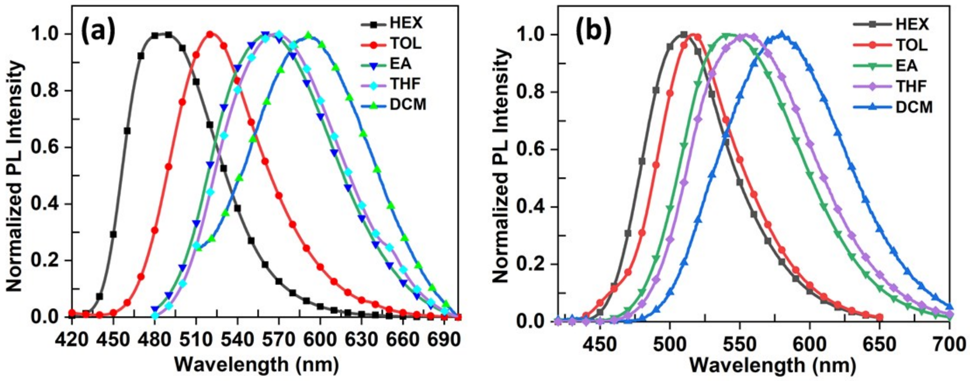

Figure S12. Fluorescence spectra (a)and (b) of **TATC-TRZ** and **TATP-TRZ** in different solvents. (HEX = *n*-hexane, TOL = toluene, DCM = dichloromethane, EA = ethyl acetate and THF = tetrahydrofuran, c = 1.0 × 10^{-5} M).

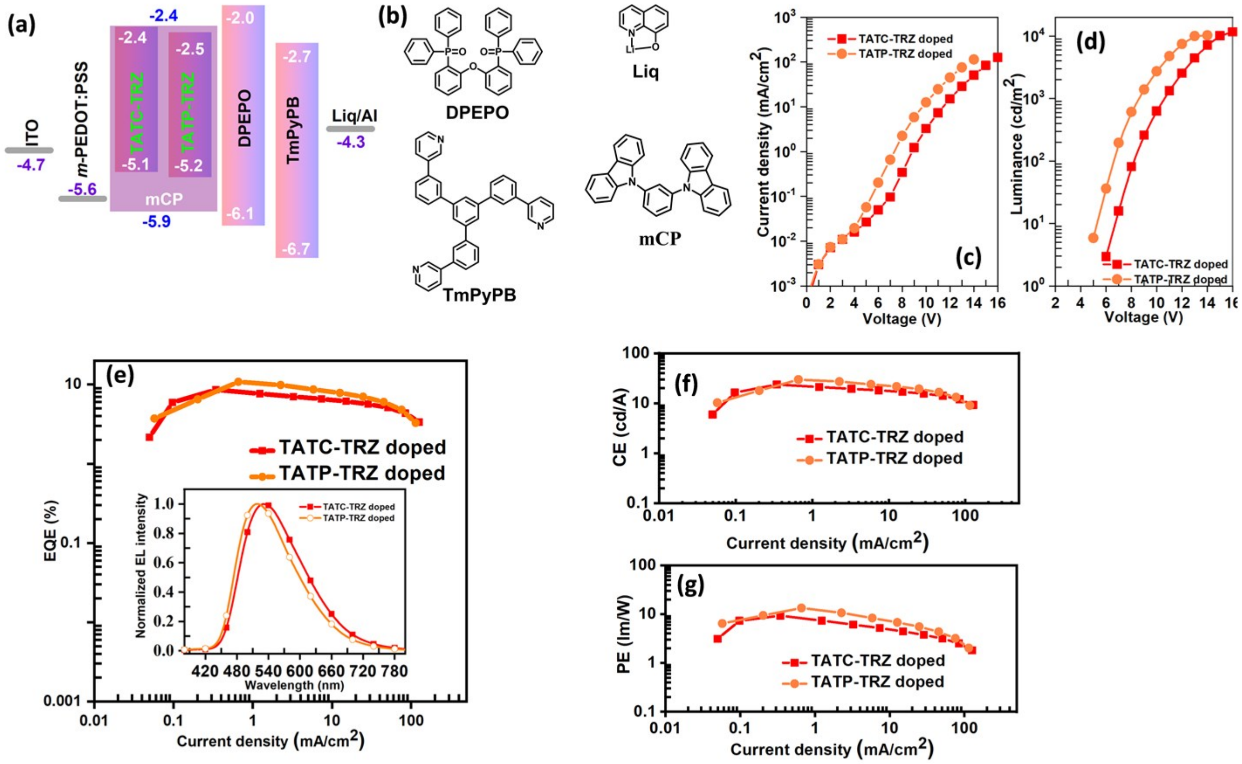

Figure S13. (a) The energy level diagrams of the doped device and (b) chemical structures of the functional materials used in the devices. (c) Current density versus voltage curves. (d) Luminance versus voltage curve. (e) External quantum efficiency versus current density curves. (Inset: normalized EL spectra of the devices. (f) Current efficiency (CE) versus current density and (g) Power efficiency (PE) versus current density of the devices.

Table S1. Photophysical characterization for two emitters of **TATC-TRZ** and **TATP-TRZ**

Compound	$\lambda_{PL}{}^{a}$ (nm)	$S_1{}^{b}$ (eV)	$T_1{}^{c}$ (eV)	$\Delta E_{ST}{}^{d}$ (eV)	$\tau_p{}^{e}$ (ns)	$\tau_d{}^{e}$ (μs)	$\Phi_{PL}{}^{f}$ (%)	$\Phi_p/\Phi_d{}^{g}$ (%)	$k_r{}^{h}$ ($10^7 s^{-1}$)	$k_{ISC}{}^{h}$ ($10^7 s^{-1}$)	$k_{RISC}{}^{h}$ ($10^7 s^{-1}$)
TATC-TRZ	526	2.72	2.71	0.01	19.9	1.4	86	0.15/0.71	0.73	4.15	0.42
TATP-TRZ	511	2.75	2.71	0.04	21.1	1.4	89	0.23/0.67	1.08	3.53	0.28

[a] Measured in doped mCP films (5 wt%) at room temperature. [b] Calculated from the onset of the fluorescence spectra of two emitters doped into mCP films (5 wt%) at 77K. [c] Calculated from the onset of the phosphorescence spectra of two emitters doped into mCP films (5 wt%) at 77K. [d] $\Delta E_{ST} = S_1{}^{b} - T_1{}^{c}$. [e] The prompt and delayed fluorescence lifetimes of two emitters doped into mCP films (5 wt%) at room temperature. [f] The total PLQYs of two emitters doped into mCP films (5 wt%) under oxygen free condition at room temperature. [g] The prompt and delayed PLQY under oxygen free conditions in mCP host film. [h] Rate constant of radiative, intersystem crossing and reverse intersystem crossing process in mCP host film.

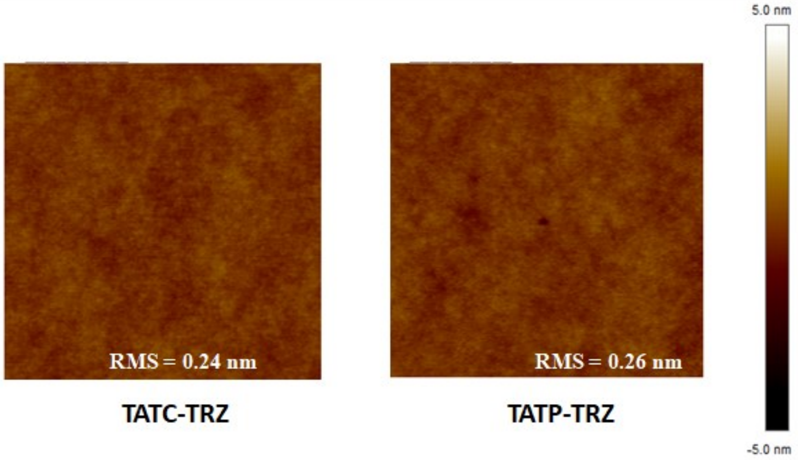

Figure S14. AFM images of **TATC-TRZ** and **TATP-TRZ** in mCP (5 wt% of emitter) doped film prepared by spin-coating with an annealing temperature of 80 °C.

Analysis of rate of constants

Time-resolved transient photoluminescence decay measurements were utilized to research the delayed fluorescence phenomenon of the molecule in neat film as shown in Figure 5. Rate constants of different kinetic processes were calculated following the equations (S1) - (S6) below:

$$k_r = \Phi_{PF} / \tau_{PF} \qquad \text{(S1)}$$

$$\Phi = k_r / (k_r + k_{nr}) \qquad \text{(S2)}$$

$$\Phi_{\mathrm{PF}} = k_{\mathrm{r}} / (k_{\mathrm{r}} + k_{\mathrm{isc}} + k_{\mathrm{nr}}) \tag{S3}$$

$$k_{risc} = k_p k_d \Phi_{\mathrm{TADF}} / k_{\mathrm{isc}} \Phi_{\mathrm{PF}} \tag{S4}$$

$$k_p = 1/\tau_{\mathrm{PF}} \tag{S5}$$

$$k_{\mathrm{d}} = 1/\tau_{\mathrm{TADF}} \tag{S6}$$

Where k_r, k_{nr}, k_{isc}, k_{risc} represent the rate constant of radiative, non-radiative, intersystem crossing and reverse intersystem crossing, respectively; $\emptyset$, $\emptyset_{PF}$, $\emptyset_{TADF}$, τ_{PF} and τ_{TADF} represent total PLQY, quantum yield of the prompt component, , lifetimes of the prompt and delayed components, respectively.